ELSEVIER

J. Non-Newtonian Fluid Mech. 2136 (2002) 1–15

Journal of Non-Newtonian Fluid Mechanics

www.elsevier.com/locate/jnnfm

Short communication

A comparison of the stress and birefringence growth of dilute, semi-dilute and concentrated polymer solutions in uniaxial extensional flows

Jonathan P. Rothstein*, Gareth H. McKinley

Department of Mechanical Engineering, Massachusetts Institute of Technology, Cambridge, MA 02139, USA

Abstract

Filament stretching experiments are used to follow the evolution in the flow-induced birefringence (FIB) and the tensile force in polymeric fluid threads undergoing uniaxial elongation. The tests are performed with several monodisperse polystyrene solutions spanning concentrations from 0.025 to 12 wt.%, and the measurements are used to investigate the extent of hysteresis in the polymeric stress and molecular conformation during imposed stretching and subsequent stress relaxation. For Deborah numbers above $De > 0.5$ (based on the longest or Zimm relaxation time), a pronounced stress-conformation hysteresis is observed in the dilute polystyrene solution at large Hencky strains, and the magnitude of the deviation from the quasi-static FENE connector force increases with imposed deformation rate. However, tests with a semi-dilute entangled polystyrene solution and a concentrated entangled polystyrene solution show that although the stress-optical rule is violated at large deformation rates and large strains, there is no evidence of any hysteresis during extension and relaxation. These observations are interpreted in terms of the relative magnitude of the stretching rate as compared to the reptation time, and also as compared to the Rouse time scales for stretching of the entire chain or for a single entangled segment. These distinct time scales depend on the number of entanglements in the fluid and govern the different relaxation mechanisms that exist in entangled polymer solutions for the polymeric stress and the molecular conformation.

Keywords: Filament stretching; Extensional rheology; Stress-conformation hysteresis

1. Introduction

A recently discovered and important dynamical feature of strong extensional flows of dilute polymer solutions is the presence of a stress-conformation hysteresis [1]. Mechanical measurements of the total polymeric stress and optical measurements of the birefringence (or polymeric deformation) during uni-

* Corresponding author. Present address: Department of Mechanical and Industrial Engineering, University of Massachusetts, Amherst, MA 01003, USA.
E-mail address: rothstei@ecs.umass.edu (J.P. Rothstein).

0377-0257/02/$ – see front matter © 2002 Elsevier Science B.V. All rights reserved.
PII: S0377-0257(02)00134-9

axial elongation show that not only is the linearity of the stress-optical rule violated, but the stress-optical coefficient, C, becomes a functional of the deformation history. When the time-dependent results are represented in a plot of polymeric stress versus molecular conformation the trajectories become loops and the stress-optical coefficient has different values during the period of externally-imposed stretching and during the subsequent free relaxation. Such hysteresis curves can be followed as a function of imposed strain and strain-rate using filament stretching rheometers coupled with polarization-state-modulated optical trains [1,2]. This stress-conformation hysteresis in strong flows is not captured by simple closed-form constitutive models such as the FENE-P dumbbell or FENE-PM chain model, but is captured by Brownian dynamics simulations of bead-rod chains, bead-spring chains and ensembles of FENE dumbbells [1,3,4]. Further details of the theoretical background, experimental techniques and computational results are available in a recently published review [5].

Recent studies have shown that the presence of a stress-conformation hysteresis is a robust feature of dilute polymer solutions in strong flows (i.e. flows having a local elongational component). Brownian dynamics simulations of exponential shear flows and planar extensional flows have demonstrated the existence of almost identical stress-conformation hysteresis loops when the results are represented in terms of the principal stresses and molecular conformations [6]. Simulations of homogeneous flows of mixed kinematics (i.e. those having both shearing and extensional components) also exhibit stress-conformation hysteresis and are described elsewhere in these proceedings. As part of this Numerical Workshop, we also described measurements of stress-conformation hysteresis in the non-homogeneous extensional flow of a dilute polymer solution flowing along the centerline of an axisymmetric contraction–expansion. Local Eulerian measurements of the velocity profile along the centerline of the contraction–expansion were used to reconstruct the deformation gradient experienced by a Lagrangian tracer particle and this strain rate profile was then provided as input to a filament stretching experiment. Simultaneous optomechanical measurement of the polymeric stress and the flow-induced birefringence (FIB) showed that beyond a critical Deborah number of $De > 0.5$ there was a measurable stress-conformation hysteresis. The extent of this hysteresis increased with strain and strain rate and correlated very well with macroscopic measurements of the enhanced pressure drop observed in flow visualization experiments [7].

A logical extension to these observations (first suggested to the authors by Prof. W. Burghardt) is to ask what happens to the stress-conformation hysteresis as the concentration of the polymeric solute is progressively increased. It has been known for a long time that in concentrated solutions the stress-optical rule becomes invalid in strong extensional flow when the molecules become significantly extended [8]. In polymer melts the stress-optical rule is usually taken to be valid up to stresses on the order of 1 MPa which—for typical molecular weights and melt temperatures—is well into the regime of non-linear viscometric properties [9,10]. These measurements and observations are based on observations in flows which are steady in an Eulerian sense. More recent measurements in transient extensional flows are reviewed in detail by Venerus et al. [11]. Measurements in polydisperse polystyrene melts have shown that the stress-optical rule remained valid during imposed stretching up to Hencky strains of four and stresses of approximately 1 MPa [11,12]. Scaling arguments based on reptation theory were used by Venerus et al. to show that the failure of the stress-optical rule is consistent with onset of significant chain stretching when the Deborah number based on the Rouse time is order one. However, in these experiments, data was not recorded during stress relaxation so it is unknown if the violation of the stress-optical rule is accompanied by stress-conformation hysteresis. In other words, is a plot of polymeric stress versus birefringence a simple function for all experimental conditions (albeit one which becomes non-linear at large stresses) or is it a functional of the total strain and strain-rate imposed on the fluid? We investigate this

question in the present short communication using simultaneous optical and mechanical measurements of the FIB and total stress in a filament stretching device on a series of solutions of increasing concentration.

2. Experimental setup

2.1. The filament stretching rheometer

Sridhar and coworkers [13,14] created the first filament stretching device capable of imposing a nearly homogeneous uniaxial extension on a fluid filament by controlling the velocity of the bottom plate while simultaneously measuring the force on the top endplate and the midpoint radius of the fluid filament. This permitted systematic measurements of the evolution in the transient extensional viscosity of the fluid filament from equilibrium to steady state extension. Many other research groups around the world have since developed filament stretching rheometers of various configurations [15].

The filament stretching rheometer (FiSER) used to make all the measurements presented in this paper is shown in Fig. 1a and follows very closely the successful design of Anna [16]. A complete description of the rheometer design and operating space can be found in [7]. In Fig. 1b, a sketch of a typical fluid filament within the FiSER is shown. Here, $L(t)$ is the time-evolving length of the filament, $R_{\mathrm{mid}}(t)$ is the midpoint radius of the filament, $F_z(t)$ is the force exerted by the filament on the endplate, $\dot{L}(t)$ is the velocity of the endplate, and L_0 and R_0 are the initial length and radius of the fluid filament. The goal of extensional rheometry is to impose a motion with a constant stretch history such that

$$\dot{\varepsilon}(t) = -\frac{2}{R_{\mathrm{mid}}(t)}\frac{\mathrm{d}R_{\mathrm{mid}}(t)}{\mathrm{d}t} = \dot{\varepsilon}_0. \tag{1}$$

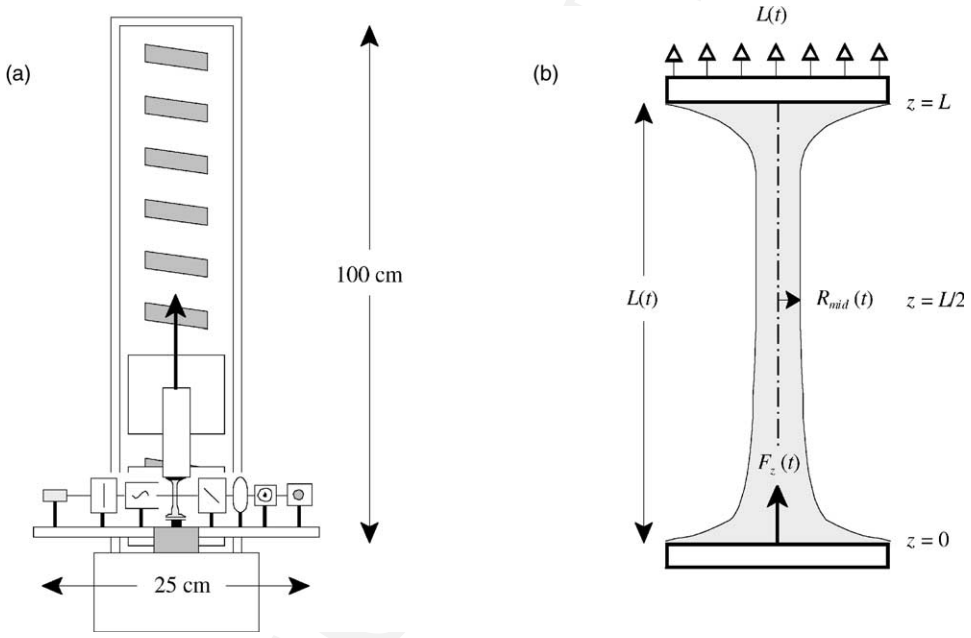

Fig. 1. Schematic diagram of (a) the FiSER and (b) a filament in mid stretch.

This is done using a master curve inversion technique [17–19] which can generate Type III test profiles from Type II [20] master curves.

The total deformation of the system can be described in terms of a Hencky strain

$$\varepsilon_{\text{eff}} = \varepsilon_D = \int_0^t \dot{\varepsilon}_{\text{eff}}(t')\,\mathrm{d}t' = -2\ln\left(\frac{R_{\text{mid}}}{R_0}\right), \tag{2}$$

while the strength of the extensional flow is characterized by the Deborah number which is the ratio of the longest characteristic relaxation time of the fluid, λ_{long}, to the characteristic timescale of the flow, $\dot{\varepsilon}_0^{-1}$,

$$De = \lambda_{\text{long}}\dot{\varepsilon}_0. \tag{3}$$

In a detailed force balance of the filament stretching rheometer, Szabo [21] showed that the principal elastic tensile stress difference generated within the filament could be calculated from the total force measured by the load cell, F_z, if the weight of the fluid, the surface tension and the inertia of the fluid are taken into account

$$\langle\tau_{zz} - \tau_{rr}\rangle = \frac{F_z}{\pi R_{\text{mid}}^2} + \frac{1}{2}\frac{\rho g(\pi L_0 R_0^2)}{\pi R_{\text{mid}}^2} - \frac{\sigma}{R_{\text{mid}}} + \frac{1}{2}\frac{\rho(\pi L_0 R_0^2)\ddot{L}_z}{\pi R_{\text{mid}}^2}, \tag{4}$$

where σ is the surface tension of the fluid, ρ the density of the fluid and $\ddot{L}_z$ the acceleration of the endplate. The last term of Eq. (4) is due to the fluid inertia and is negligibly small for the present experiments. The principal elastic tensile stress can be further broken down into contributions from the polymer and its Newtonian solvent

$$\langle\tau_{zz} - \tau_{rr}\rangle = \Delta\tau_{\text{p}} + 3\eta_{\text{s}}\dot{\varepsilon}, \tag{5}$$

The transient extensional viscosity of polymeric fluids in homogenous uniaxial extension

$$\eta_{\text{E}}{}^{+} = \frac{\langle\tau_{zz} - \tau_{rr}\rangle}{\dot{\varepsilon}_0} = 3\eta_{\text{s}} + \frac{\Delta\tau_{\text{p}}}{\dot{\varepsilon}_0}. \tag{6}$$

The Trouton ratio is defined as $Tr = \eta_{\text{E}}^{+}/\eta_0$.

2.2. Flow-induced birefringence

The molecular polarizability and hence the macroscopic refractive index of a typical linear homopolymer chain is different in the directions parallel to and normal to the chain backbone [10]. FIB measurements have been used quite extensively to examine steady and transient flows of polymeric fluids [1,9–11]. By passing light of a known polarization state and frequency through the polymeric fluid sample and measuring the resulting change in polarization state, FIB can be used to determine the local anisotropy in the conformation of the polymer chains [10]. In a homogeneous uniaxial extensional flow the resulting expression for the birefringence is

$$\frac{\Delta n'}{C} = G\Delta A, \tag{7}$$

where $\Delta n'$ is the measured birefringence, C the stress-optical coefficient, G the characteristic elastic modulus of the fluid, and $\Delta A = A_{11} - A_{22}$ is a measure of the anisotropy in the average conformation of the

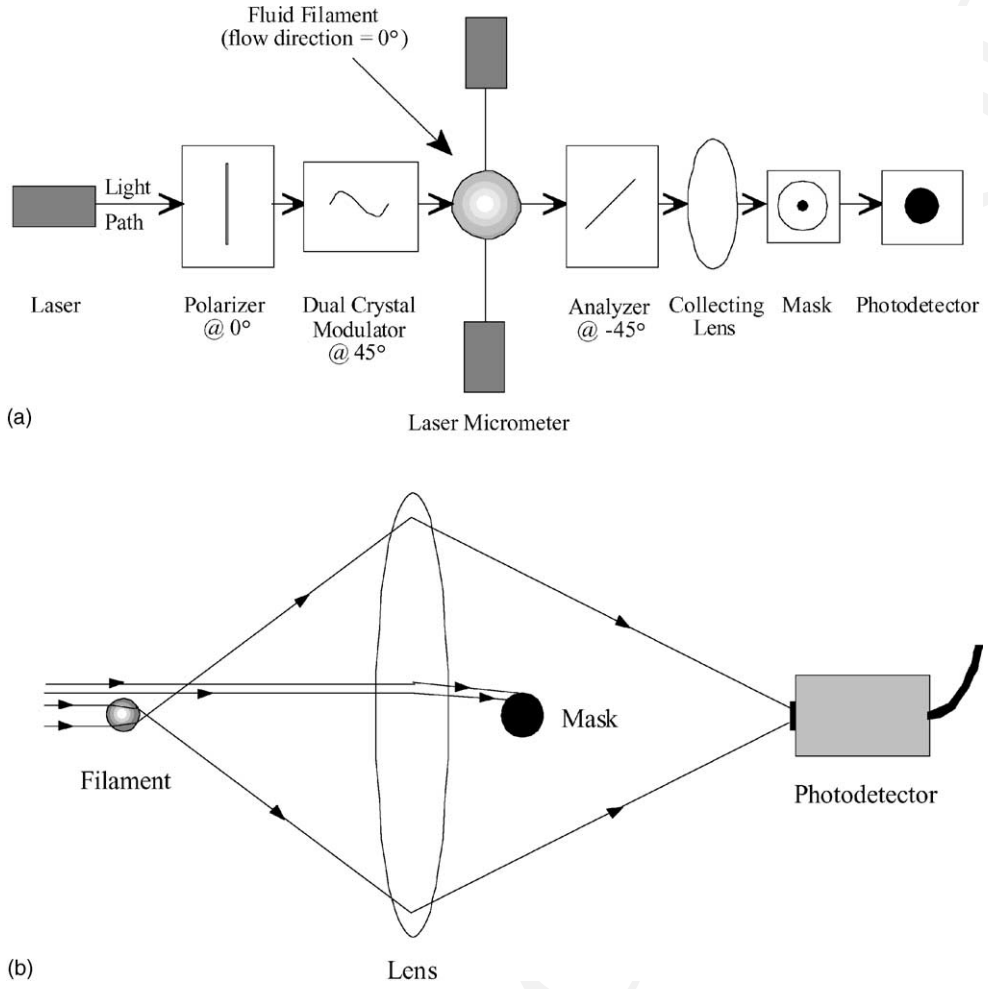

Fig. 2. Schematic diagram in the (x, y) plane of (a) the FIB optical train and (b) the masking technique.

polymer chain. The polymer conformation is characterized by the ensemble average dimensionless second moment tensor, $\boldsymbol{A} = \langle \boldsymbol{QQ} \rangle / Q_{eq}^2$, where $\boldsymbol{Q}$ is the end-to-end vector of the polymer chain. For the dilute solution $G = nk_B T = cNk_B T/M_w$ and for the entangled solutions $G = G_N^0$ is the plateau modulus of the fluid.

The optical path for the polarization modulated flow birefringence system employed in this research is shown in Fig. 2a and is similar in design to the modulated system pioneered by Frattini and Fuller [22]. The system is light, insensitive to mechanical vibration and can be successfully mounted to the lower platen of the FiSER where it can measure the birefringence at the midpoint of the filament as it is stretched. The polarized laser light is generated by a 4.5 mW, 635 nm laser diode (Thorlabs CPS43AP05ME). The light is first passed through a linear polarizer (New Focus 5524) oriented at 0° from the vertical axis of the filament stretching rheometer. The polarized light is then sent through a dual-crystal electro-optical modulator oscillating at 44 kHz and oriented at -45°. Finally, the light passes through a biconvex collecting lens (Newport KBX39) and a mask before it is collected on a photodetector (Thorlabs PDA55).

There are several major difficulties associated with successfully taking optical measurements of a thinning fluid column in a FiSER [7]. The radial curvature of the filament acts like a cylindrical lens, fanning the laser light and dramatically reducing the intensity of the light reaching the photodetector. As the filament shrinks, the magnitude of the light spreading will increase. Depending on the axial strain imposed, the filament may become smaller than the cross section of the incoming laser beam and allow laser light which has passed around the filament to reach the photodetector. A solution to both of these problems was presented by Talbott [23] and is demonstrated in Fig. 3b. A lens is placed such that the diverging light exiting the filament (which acts as a cylindrical lens) is refocused onto the photodetector. The light that passes around the filament is not spread and is blocked by the mask which for our experiments is composed of a black cylindrical rod of diameter, $d_{\text{mask}} = 2.0\,\text{mm}$. By mounting the mask directly behind the collecting lens, only a small amount of light which has passed through the filament is blocked.

At the onset of filament stretching, the no slip condition at the endplates and the sagging due to gravity can result in strong axial curvature of the filament. The degree of off-axis vertical deflection of the laser beam is a complicated function of the stretch rate, the fluid properties and the initial loading of the sample and is difficult to correct for optically. The lateral position of the filament can also shift slightly due to air currents, slight misalignment of the rheometer or mechanical vibration. To lessen the impact of both these problems a large area photodetector ($3\,\text{mm} \times 3\,\text{mm}$) was used. The advantage of this large area photodetector is a reduced sensitivity to the lateral filament location and axial curvature. The disadvantage is an enhanced sensitivity to ambient light which must then be minimized.

By using a modulation technique, it is possible to calculate both the retardation, $\delta = (2\pi\Delta n'\mathrm{d})/\lambda_{\text{light}}$, and the extinction angle, χ, simultaneously from the first and second harmonic of the modulated laser intensity

$$\delta = \frac{4\pi\Delta n' R_{\text{mid}}(t)}{\lambda_{\text{light}}} = \cos^{-1}\left(\frac{-M_{32}^2 \pm M_{34}^2\sqrt{1 - M_{34}^2 - M_{32}^2}}{M_{34}^2 + M_{32}^2}\right), \qquad \chi = \frac{1}{2}\cos^{-1}\left(\frac{M_{34}}{\sin\delta}\right). \tag{8}$$

where the optical path-length equal to $d = 2R_{\text{mid}}(t)$, λ_{light} is the wavelength of the laser light and M_{34} and M_{32} are the components of the Mueller matrix corresponding to the optical train shown in Fig. 2a. These can be determined from measurements of the time varying light intensity

$$M_{34} = \frac{I_\omega}{2J_1(A_c)I_{\text{dc}}}, \qquad M_{32} = \frac{I_{2\omega}}{2J_2(A_c)I_{\text{dc}}}. \tag{9}$$

In Eq. (9), A_c is the amplitude of the electro-optical modulation calibrated such that the order zero Bessel function of the first kind is equal to $J_0(A_c) = 0$ [22] and the intensity of the light measured by the photodetector is given by

$$I(t) = I_{\text{dc}} + I_\omega \sin\omega t + I_{2\omega}\cos 2\omega t. \tag{10}$$

For the uniaxial deformation considered in the present study, the orientation angle is $\delta = 0$ for all experiments and the minimum resolvable retardation of this system is approximately $\delta \approx 1 \times 10^{-2}\,\text{rad}$.

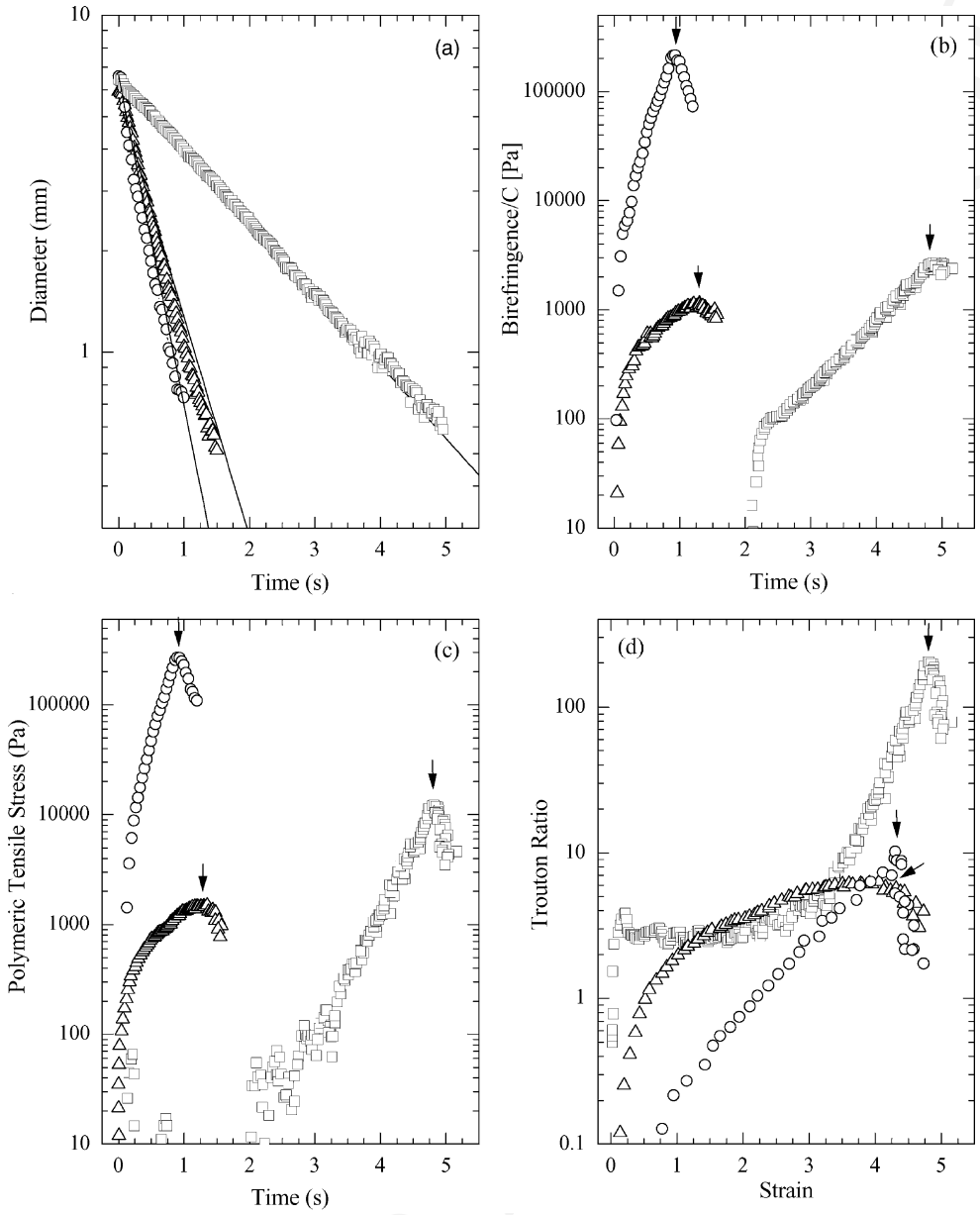

Fig. 3. Representative plots of (a) diameter, (b) birefringence, (c) polymeric tensile stress and (d) Trouton ratio for filament stretching experiments of fluids PS025, PS5 and PS12. The data include: (○) experimental data of PS12 at a Deborah number of $De = 69.8$ ($\dot{\varepsilon} = 4.5\,s^{-1}$) to a final Hencky strain of $\varepsilon_f = 4.5$; (△) experimental data of PS5 at a Deborah number of $De = 5.0$ ($\dot{\varepsilon} = 3\,s^{-1}$) to a final Hencky strain of $\varepsilon_f = 4.5$; and (□) experimental data of PS025 at a Deborah number of $De = 4.1$ ($\dot{\varepsilon} = 1\,s^{-1}$) to a final Hencky strain of $\varepsilon_f = 4.7$. The arrows indicate the start of relaxation for each experiment.

Table 1
Parameters characterizing the viscometric properties of the three monodisperse polystyrene test fluids

Parameter	Description	PS12	PS5	PS025
c (%)	Concentration of polystyrene	12	5	0.025
c/c^*	Fraction of critical entanglement concentration	70	33	0.24
M_w/M_n	Polydispersity	1.13	1.08	1.03
M_w	Molecular weight (g/mol)	1.96×10^6	2.0×10^6	2.0×10^6
$M_{e,soln}$	Molecular weight between entanglements (g/mol)	1.31×10^5	4.32×10^5	–
$Z = M_w/M_{e,soln}$	Entanglements per polymer chaing	15	5.4	
$b = L^2$	Extensibility parameter	528	1467	7921
G	Elastic modulus (Pa)	2.21×10^3	278	0.98
η_0	Zero shear rate viscosity (Pa s)	6.93×10^3	60.9	22.75
η_s	Solvent viscosity (Pa s)	0.01	0.01	21
λ_d	Reptation or disentanglement time (s)	13	2.6	–
λ_{Rouse}	Rouse time for relaxation of entire chain (s)	0.53	0.49	–
λ_e	Rouse time for relaxation between entanglement points (s)	0.0023	0.017	–
λ_z	Zimm relaxation time (s)	–	–	3.24

The relaxation times for the entangled fluids are determined by fitting the linear viscoelastic data $\{G'(\omega), G''(\omega)\}$ to the tube model of Milner and McLeish [31] incoporating chain length fluctuations. Further details are provided in [19].

2.3. Description of test fluids

Three different solutions of high molecular weight, monodisperse polystyrene (PS) (Scientific Polymer Products Inc.) were used as test fluids in the experiments presented in this paper. The first test fluid (PS025) is a dilute polymer solution consisting of 0.025 wt.% PS dissolved in oligomeric styrene (Hercules). The second fluid (PS5) is a semi-dilute entangled solution of 5% PS in tricreslyphospate solvent (TCP) (Aldrich) prepared in our laboratory [24]. The third fluid (PS12), is a concentrated entangled solution of 12% PS in TCP prepared by Venerus and Kahvand [25]. The viscometric functions characterizing these fluids have been published previously and will not be reproduced here [19,24–26]. A summary of the important rheological parameters for the test fluids is presented in Table 1. These viscometric parameters were calculated by fitting small amplitude oscillatory shear flow data to a Rouse–Zimm model in the case of the dilute polymer solution and the Doi–Edwards model incorporating contour length fluctuations in the case of the semi-dilute and concentrated polymer solutions. For each test fluid, the stress-optical coefficient is assumed to be $C = -5.0 \times 10^{-9}\,\mathrm{Pa}^{-1}$. This is consistent with the values found in the literature for polystyrene which typically range between $-4.0 \times 10^{-9} < C < -6.0 \times 10^{-9}\,\mathrm{Pa}^{-1}$ [1,9,11].

3. Results and discussion

To compare the results of transient homogeneous uniaxial extension for the three fluids directly, representative plots of filament diameter, birefringence, elastic tensile stress and Trouton ratio are presented in Fig. 3. The data in each subfigure include experimental measurements for the PS025, PS5 and PS12 fluids at Deborah numbers of $De = 4.1$, 9.6 and 69.8 and final Hencky strains of $\varepsilon_f = 4$, 4.5 and 4.5, respectively. In Fig. 3a, the diameter of the fluid filaments are presented as a function of time. A line corresponding to an ideal Type III stretch profile is also included for comparison to each experiment.

A homogeneous deformation is achieved for all three test fluids. This is the case, not just for the three representative experiments presented in Fig. 3, but for all the experiments presented in this study. The birefringence divided by the stress-optical coefficient, $\Delta n'/C$ is shown as a function of time in Fig. 3b. At short times, the birefringence signal is extremely small for the dilute PS025 test fluid $\Delta n' \leq 10^{-8}$. At these small strains, the tensile stress in the dilute solution is dominated by the response of the Newtonian solvent and one does not expect to see significant orientation or extension of the polymer chains. As time progresses and the accumulated Hencky strain increases beyond $\varepsilon > 2$, the birefringence signal becomes measurable and begins to grow exponentially with time. The birefringence growth agrees quite well with the prediction of FENE-PM models [7]. For the semi-dilute, PS5, and the concentrated, PS12, solutions, the birefringence begins to grow quickly with the onset of stretching. The birefringence signals increase in intensity with increasing concentration of the high molecular weight polymer.

The trends in the growth of the polymeric tensile stress presented in Fig. 3c are similar to those observed for the growth of the birefringence. The one major distinction is that the polymeric tensile stress measured for the dilute elastic test fluid, PS025, demonstrates considerable strain hardening. This is perhaps more easily observed in the Trouton ratios presented in Fig. 3d. As has been observed previously for dilute polymer solutions [15], the Trouton ratio for the PS025 test fluid increases quickly from zero, remaining near a value of $Tr \approx 3$ until a Hencky strain of approximately $\varepsilon \approx 3$. At this point, significant strain hardening begins. The plateau at early strains is caused by the large solvent contribution to the tensile stress. This plateau is not observed in either PS5 or PS12 because the solvent viscosity is a much smaller fraction of the zero shear rate viscosity and, at short times, the responses in these entangled solutions is dominated by linear viscoelastic effects. The slow growth of the Trouton ratio and limited strain hardening in these entangled systems is consistent with linear viscoelastic theory and previous experiments [19,24].

In Fig. 4, the polymeric contribution to the tensile stress is plotted against the polymer coil conformation for the homogeneous transient uniaxial extension experiments of the dilute polymer solution, PS025. The polymer contribution to the tensile stress is calculated from Eq. (5) while the ensemble average conformational anisotropy of the polymer chains is determined by an algebraic manipulation of Eq. (7)

$$\Delta A = \frac{1}{GC}\left(\frac{\delta\lambda_{\text{light}}}{4\pi R_{\text{mid}}}\right). \tag{11}$$

For convenience, we refer to ΔA as the 'polymer conformation' henceforth. The stretch and subsequent relaxation of two different experiments is shown in Fig. 4. The experiments were performed at two different Deborah numbers based on the longest relaxation time, $De = \lambda_z\dot{\varepsilon}_0 = 4.1$ and $De = 8.2$, and were terminated at the same final Hencky strain, $\varepsilon = 4$. At Deborah numbers above the coil-stretch transition, $De > 0.5$, one expects to see considerable strain hardening in the fluid. Both experiments demonstrate a dramatic stress-conformation hysteresis comparable in size to the hysteresis loops first observed by Doyle et al. [1] and later by Sridhar et al. [2] for dilute polymer solutions. During the imposed stretching, the data follows the upper branch of the loop while during relaxation the data follow the lower branch of the hysteresis loop. The polymer conformation in each experiment grows to a value of approximately $\Delta A \approx 1000$ before the stretch is stopped. The extent of chain orientation and unraveling is found to be almost independent of rate of deformation and only dependent on the total accumulated strain. The polymeric stress, however, is found to be approximately linearly dependent on the strain rate. This same observation has been made in the transient extensional rheology literature where the Trouton ratio has been shown to be independent of Deborah number above a Deborah number of $De \approx 1$ [15].

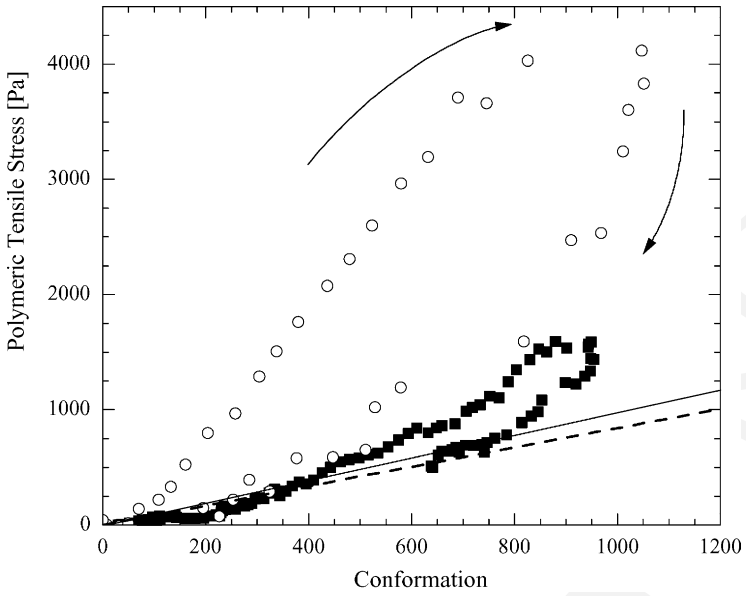

Fig. 4. Polymeric tensile stress as a function of polymer coil conformation for a filament stretching experiment of the 0.025 wt.% PS/PS solution to a final Hencky strain of $\varepsilon_f = 4$. The data include: (○) experimental data at a Deborah number of $De = 8.2$; (■) experimental data at a Deborah number of $De = 4.1$; (—) FENE-PM model fit; and (- - -) Gaussian chain fit.

The solid curve shows the value expected from FENE-PM spring theory

$$\frac{\Delta\tau_p}{\Delta A} = G\frac{1}{1 - tr\{\boldsymbol{A}\}/L^2}. \tag{12}$$

The FENE-PM model does not qualitatively capture the hysteresis loop because it does not capture information about the internal configurations of the chains and the non-linear spring connector is a single valued function of the polymer conformation [1]. Both experiments relax along the same path, approaching the FENE-PM predictions, suggesting that there is a universal relaxation process independent of strain and strain rate.

Detailed analyses of Brownian dynamics computations show that stress-optical hysteresis in dilute polymer solutions arises due to a constriction in the phase space that can be explored by polymer chains undergoing rapid stretching at deformation rates $\dot{\varepsilon}_0 > \lambda_{Zimm}^{-1}$ [1,4]. Because each chain is unable to sample the full phase space available to it at a given strain, the net tensile force in the chain is not well described by expressions such as the inverse Langevin or FENE connector force law. These quasi-equilibrium expressions are derived from the most probable configurations of kinetic theory at a given strain. Instead, the individual polymer chains are predisposed to evolve through a limited number of distinctive non-equilibrium conformations based on their initial configuration at the onset of stretching [27]. Recently, Ghosh et al. have proposed an adaptive length scale (ALS) model in which the polymer chain is decomposed into a number of identical shorter segments [28]. The number of such segments is governed by the total strain and by the flow strength, so that on the scale of the individual segment (with time constant λ_e) the flow is weak enough that the segments are well described by existing dumbbell kinetic theory i.e. ($\dot{\varepsilon} < 1/\lambda_e$). Computations using this model indicate that it is able to describe, at least qualitatively, many features

of complex flows of dilute solutions at high Deborah numbers including the enhanced pressure drop in axis-symmetric contraction–expansions and the stability of flow past cylinders [29]. The measurements described in the present note can also be understood within the context of such segment-level models.

A set of homogeneous transient uniaxial elongation experiments was also performed on the semi-dilute entangled solution PS5. The results of three experiments at Deborah numbers based on reptation or 'disengagement' time, λ_d, of $De = \lambda_d \dot{\varepsilon}_0 = 9.6$, 16.1 and 23.7 to a final Hencky strain of $\varepsilon_f = 4.5$, 4.5 and 6.0, respectively are shown in Fig. 5. Although the birefringence measured in for the PS5 fluid is much larger than that observed for the PS025 fluid, the conformational anisotropy computed using Eq. (7) is much smaller due to the greater number density of polymer chains and the 300-fold increase in the plateau modulus (see Table 1). The maximum conformational anisotropy achieved by the polymer chains of the PS5 is $\Delta A_{max} \approx 90$. For an entangled fluid, the extensibility of each entangled segment (L^2_{seg}) is reduced from the value for the whole chain by a factor of $Z = M_w/M_{e,soln}$. The chain conformation and polymeric stress should thus be related by an expression of the form

$$\Delta\tau_p = G\frac{1}{1 - tr\{\boldsymbol{A}\}/(L^2/Z)}\Delta A. \tag{13}$$

The data in Fig. 5 show that as the strain rate is increased the maximum values of the polymeric stress and maximum conformational anisotropy increase. However, the data is always well described by the

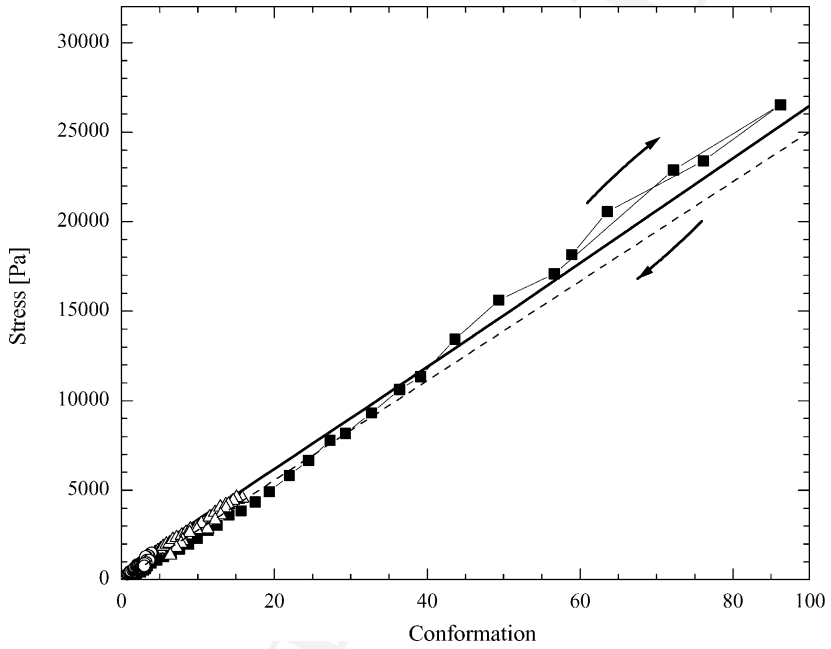

Fig. 5. Polymeric tensile stress as a function of polymer coil conformation for a filament stretching experiment of fluid PS5. The data include: (■) experimental data at a Deborah number of $De = 23.7$ to a final Hencky strain of $\varepsilon_f = 6.0$; (○) experimental data at a Deborah number of $De = 9.6$ to a final Hencky strain of $\varepsilon_f = 4.5$; (△) experimental data at a Deborah number of $De = 16.1$ to a final Hencky strain of $\varepsilon_f = 4.5$; (—) FENE-PM model fit; and (- - -) Gaussian chain fit. The difference between the FENE-PM and the Gaussian chain fit arises because $\Delta A = (A_{22} - A_{11})$ and $TrA = A_{11} + 2A_{22}$ are not equivalent for small deformations when the A_{22} contribution is not negligibly small.

FENE connector force (Eq. (12)). There is no evidence of stress-conformation hysteresis during uniaxial stretching for the range of strains and strain rates explored. The stress-optical rule is found to be invalid at stresses on the order of $\Delta\tau_p \approx 15000$ Pa and a total accumulated Hencky strain of $\varepsilon \approx 5$ for this semi-dilute entangled polymer solution.

Although the Deborah number for each of these filament stretching experiments is well above $De > 0.5$, none of these experiments demonstrate a measurable stress-conformation hysteresis. Recall that we have defined the Deborah number using the longest relaxtion time of the fluid. In this case, the Deborah number is evaluated using the reptation time, λ_d. However, in entangled systems there are several important distinctive timescales [30,31] including the reptation time, λ_d, the Rouse time for chain stretching within the entire tube, λ_{Rouse}, and the 'equilibration time' or Rouse time for relaxation of the chain between entanglement points. The original reptation theory for a well-entangled system with Z entanglements per chain gives $\lambda_{Rouse} = Z^2\lambda_e$ and $\lambda_d = 3Z\lambda_{Rouse}$ [30]. A more refined theory incorporating chain-length fluctuations (or 'breathing modes') for moderately entangled systems indicates that $\lambda_d \cong \lambda_{Rouse}3Z(1 - 1/\sqrt{Z})^2$ [31].

The values for each of these relaxation times for the PS5 and PS12 fluids can be found in Table 1. In Table 2 we re-evaluate the Deborah number for each homogeneous uniaxial extension experiment using the different relaxation times of PS5. From Table 2 we see that the two highest strain rates presented in Fig. 5 are above a Deborah number of $De > 0.5$ when the Deborah number is evaluated using either the reptation time or the Rouse time of the chain, but are both well below this critical value when the Deborah number is evaluated using the Rouse time corresponding to relaxation of the polymer chain between entanglement points. The weak deviation of the force-conformation curve shown in Fig. 5 is consistent with the onset of chain stretching at $De_{Rouse} > 0.5$. However, the absence of stress-conformation hysteresis for this semi-dilute entangled solution suggests that the strain rate needs to be large enough to result in strong non-equilibrium conformation of the polymer chain between entanglement points. To realize a flow with $De_e = \lambda_e\dot{\varepsilon} > 0.5$ would require strain rates of $\dot{\varepsilon}_0 \geq (0.5/\lambda_e) \approx 29.4\,s^{-1}$ Such deformation rates are not presently attainable in our filament stretching rheometers.

In Fig. 6 the results of the homogeneous uniaxial extension of the concentrated entangled polymer solution PS12 are shown for Deborah numbers of $De = \lambda_d\dot{\varepsilon}_0 = 16.2$ to a final Hencky strain of $\varepsilon = 5.5$ and 6.0, respectively. No significant stress-conformation hysteresis is observed in this case even though the fluid does exhibit some strain hardening and violates the stress-optical rule at a polymeric tensile stress of approximately $\Delta\tau_p \approx 50{,}000$ Pa. Large polymeric tensile stresses are measured as the fluid filament undergoes a relatively large conformation change of $\Delta A_{max} \approx 100$ corresponding to approximately 20% of the maximum extensibility of the entangled PS12 solution. This strain rate corresponds to Deborah numbers of $De_d = 69.8$, $De_{Rouse} = 2.84$ and $De_e = 0.012$. Although chain

Table 2
Deborah numbers of the experiments in Fig. 5 evaluated using the different characteristic relaxation times of the semi-dilute PS5 solution

Strain rate (s^{-1})	$De_d = \lambda_d\dot{\varepsilon}_0$	$De_{Rouse} = \lambda_{Rouse}\dot{\varepsilon}_0$	$De_e = \lambda_e\dot{\varepsilon}_0$
1.3	3.4	0.65	0.022
3.7	9.6	1.8	0.063
6.2	16.1	3.1	0.11
9.1	23.7	4.5	0.15

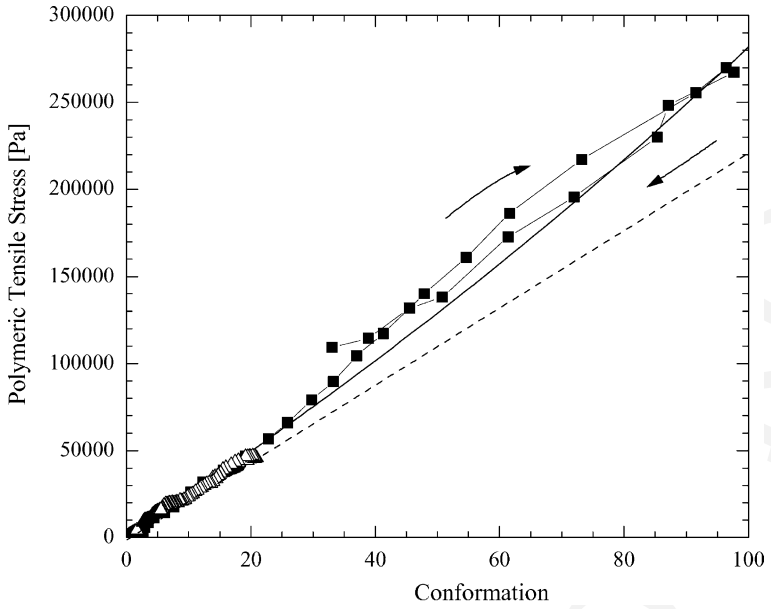

Fig. 6. Polymeric tensile stress as a function of polymer coil conformation for a filament stretching experiment of fluid PS12. The data include: (■) experimental data at a Deborah number of $De = 69.8$ to a final Hencky strain of $\varepsilon_f = 6.0$; (△) experimental data at a Deborah number of $De = 16.2$ to a final Hencky strain of $\varepsilon_f = 5.5$; (—) FENE-PM model fit; and (- - -) Gaussian chain fit.

stretching is observed, the flow is weak on the scale of the Rouse time for relaxation between entanglement points, λ_e.

4. Summary and discussion

In the present note, we have used simultaneous optical and mechanical measurements of the birefringence and tensile force to probe the stress-conformations response of polymeric fluids undergoing transient uniaxial elongation. In contrast to measurements in dilute polymer solutions there is no evidence of stress-conformation hysteresis for the semi-dilute or concentrated entangled solutions. On the basis of these observations, coupled with other recently published data [11,19,32] and numerical calculations [33,34], three distinct regimes can be identified:

- For $\lambda_d\dot{\varepsilon} < 0.5$ steady state Trouton ratio of $Tr = 3$ is obtained.
- At intermediate deformation rates, $0.5, < \dot{\varepsilon}_0\lambda_d < (\lambda_d/\lambda_{Rouse})$ tube orientation results in extension-rate thinning and a monotonic decrease in the steady state extensional viscosity, but the polymer chain within the tube is not stretched.
- At higher deformation rates, $(\lambda_d/\lambda_{Rouse}) < \dot{\varepsilon}_0\lambda_d$ chain stretching within the oriented segments leads to strain-hardening in transient uniaxial extension and a progressive failure of the stress-optical rule. However, the force law is still well described by a non-linear FENE-type connector force.

Recent theoretical considerations have shown that the validity of the stress-optical rule is quite general [35] provided that there is only deformation of the constraining tubes and no stretching of the chain

contained within. For flows of high Deborah numbers, corresponding to stretch rates $\dot{\varepsilon}_0 > \lambda_{\text{Rouse}}^{-1}/2$ the combined optomechanical measurements show chain stretching leads to a non-linear relationship between the polymer stress and FIB. The present results are consistent with the observations of Venerus et al. [11] in polystyrene melts; however, our values of the polymeric stress at which the deviation from linearity is observed are much lower due to the lower polymer concentration and the lower number of entanglements of the polymer solutions tested.

Although we can monitor the progressive failure of the stress-optical rule at high strains we do not observe stress-conformation hysteresis in the entangled solutions. Although the flow generated in the filament stretching device is strong on the scale of the overall chain, it is weak on the level of the individual segment because $\lambda_e\dot{\varepsilon}_0 < 0.5$ or, equivalently, $\lambda_d\dot{\varepsilon}_0 < 1.5Z^3(1-1/\sqrt{Z})^2$.

We thus expect that the internal degrees of freedom of each chain segment will have sufficient time to sample their full phase-space during elongation, thus leading to a force law that is well described by quasi-equilibrium kinetic theory, and the absence of a stress-orientation hysteresis. In order to observe such hysteresis one would need to generate 'kinked' configurations within each segment, and this would require a very strong flow, $\lambda_d\dot{\varepsilon}_0 > (\lambda_d/\lambda_e) \approx 1.5Z^3(1-1/\sqrt{Z})^2$. Using the information in Table 1 and this criterion we can estimate that for PS12 we would require $De = \lambda_d\dot{\varepsilon}_0 > 2786(\dot{\varepsilon}_0 > 215\,\text{s}^{-1})$ and for PS5 we would require $De = \lambda_d\dot{\varepsilon}_0 > 77(\dot{\varepsilon}_0 > 29\,\text{s}^{-1})$. However, it should be noted that further studies are needed to determine if, even at these high Deborah numbers, a stress-conformation hysteresis exists for semi-dilute and concentrated polymer solutions in homogeneous uniaxial extensional flows. In particular, it is possible that convective constraint release in a rapid extensional flow will also substantially modify the local transient stretching of the chain segments in concentrated solutions.

Acknowledgements

The work described in this short communication was motivated in part by a question raised by Prof. W. Burghardt during the course of the XIIth International Workshop on Numerical Methods in Viscoelastic Flows. This research was supported by NASA under grant NAG3-1793 and by a gift from the Schlumberger Foundation.

References

[1] P.S. Doyle, E.S.G. Shaqfeh, G.H. McKinley, S.H. Spiegelberg, Relaxation of dilute polymer solutions following extensional flow, J. Non-Newtonian Fluid Mech. 76 (1998) 79–110.
[2] T. Sridhar, D.A. Nguyen, G.G. Fuller, Birefringence and stress growth in uniaxial extension of polymer solutions, J. Non-Newtonian Fluid Mech. 90 (2000) 299–315.
[3] R. Sizaire, G. Lielens, I. Jaumain, R. Keunings, V. Legat, On the hysteretic behavior of dilute polymer solutions in relaxation following extensional flow, J. Non-Newtonian Fluid Mech. 82 (1999) 233–253.
[4] I. Ghosh, G.H. McKinley, R.A. Brown, R.C. Armstrong, Deficiencies of FENE dumbbell models in describing the rapid stretching of dilute polymer solutions, J. Rheol. 45 (2001) 721–758.
[5] G.H. McKinley, T. Sridhar, Filament stretching rheometry, Annu. Rev. Fluid Mech. 34 (2002) 375–415.
[6] T.C.B. Kwan, N.J. Woo, E.S.G. Shaqfeh, An experimental and simulation study of dilute polymer solutions in exponential shear flow: comparison to uniaxial and planar extensional flows, J. Rheol. 45 (2001) 321–349.
[7] J.P. Rothstein, G.H. McKinley, Non-homogeneous transient uniaxial rheometry, J. Rheol., submitted for publication.
[8] W.H. Talbott, J.D. Goddard, Streaming birefringence in extensional flows of polymer solutions, Rheol. Acta 18 (1979) 505–517.

[9] H. Janeschitz-Kriegl, Polymer Melt Rheology and Flow Birefringence, Springer-Verlag, Berlin, 1983.
[10] G.G. Fuller, Optical Rheometry of Complex Fluids, Oxford University Press, New York, 1995.
[11] D.C. Venerus, S.H. Zhu, H.-C. Ottinger, Stress and birefringence measurements during the uniaxial elongation of polystyrene melts, J. Rheol. 43 (1999) 795–813.
[12] T. Kotaka, A. Kojima, M. Okamoto, Elongational flow opto-rheometry for polymer melts. 1. Construction of an elongational flow opto-rheometer and some preliminary results, Rheol. Acta 36 (1997) 646–656.
[13] V. Tirtaatmadja, T. Sridhar, A filament stretching device for measurement of extensional viscosity, J. Rheol. 37 (1993) 1133–1160.
[14] T. Sridhar, V. Tirtaatmadja, D.A. Nguyen, R.K. Gupta, Measurement of extensional viscosity of polymer solutions, J. Non-Newtonian Fluid Mech. 40 (1991) 271–280.
[15] S.L. Anna, G.H. McKinley, D.A. Nguyen, T. Sridhar, S.J. Muller, J. Huang, D.F. James, An inter-laboratory comparison of measurements from filament stretching rheometers using common test fluids, J. Rheol. 45 (2001) 83–114.
[16] S.L. Anna, Filament stretching of model elastic liquids, Ph.D. Thesis, Division of Engineering and Applied Sciences, Harvard University, 2000.
[17] N.V. Orr, T. Sridhar, Probing the dynamics of polymer solutions in extensional flow using step strain rate experiments, J. Non-Newtonian Fluid Mech. 82 (1999) 203–232.
[18] S.L. Anna, C.B. Rogers, G.H. McKinley, On controlling the kinematics of a filament stretching rheometer using a real-time active control mechanism, J. Non-Newtonian Fluid Mech. 87 (1999) 307–335.
[19] G.H. McKinley, O.F. Brauner, M. Yao, Kinematics of filament stretching in dilute and concentrated polymer solutions, Korea Aust. Rheology J. 13 (2001) 29–35.
[20] M.I. Kolte, H.K. Rasmussen, O. Hassager, Transient filament stretching rheometry. II. Numerical simulation, Rheol. Acta 36 (1997) 285–302.
[21] P. Szabo, Transient filament stretching rheometry. I. Force balance analysis, Rheol. Acta 36 (1997) 277–284.
[22] P.L. Frattini, G.G. Fuller, A note on phase-modulated flow birefringence, J. Rheol. 28 (1984) 61–70.
[23] W.H. Talbott, Streaming birefringence in extensional flow of polymer solutions, Ph.D. Thesis, University of Michigan, 1978.
[24] O.F. Brauner, Steady spinning of synthetic silk-like fibers and transient filament stretching of semi-dilute and concentrated polymeric fluids, M.S. Thesis, Chemical Engineering, Massachusetts Institute of Technology, 2001.
[25] D.C. Venerus, H. Kahvand, Doi–Edwards theory evaluation in double-step strain flows, J. Polym. Sci. Part B 32 (1994) 1531–1542.
[26] J.P. Rothstein, G.H. McKinley, The axisymmetric contraction–expansion: The role of extensional rheology on vortex growth dynamics and the enhanced pressure drop, J. Non-Newtonian Fluid Mech. 98 (2001) 33–63.
[27] L. Li, R.G. Larson, T. Sridhar, Brownian dynamics simulations of dilute polystyrene solutions, J. Rheol. 44 (2000) 291–322.
[28] I. Ghosh, Y.L. Joo, G.H. McKinley, R.A. Brown, R.C. Armstrong, A new model for dilute polymer solutions in flows with strong extensional components, J. Rheol., submitted for publication.
[29] Y.L. Joo, M.D. Smith, R.C. Armstrong, R.A. Brown, Linear stability analysis of flow of an Oldroyd-B fluid through a linear array of cylinders, J. Non-Newtonian Fluid Mech., submitted for publication.
[30] M. Doi, S.F. Edwards, The Theory of Polymer Dynamics, Oxford University Press, Oxford, 1986.
[31] S.T. Milner, T.C.B. McLeish, Reptation and contour-length fluctuations in melts of linear polymers, Phys. Rev. Lett. 81 (1998) 725–728.
[32] P.K. Bhattacharjee, J. Oberhauser, G.H. McKinley, L.G. Leal, T. Sridhar, Extensional rheometry of entangled solutions, Macromolecules, submitted for publication.
[33] G. Marrucci, N. Grizzuti, Fast flows of concentrated polymers: predictions of the tube model on chain stretching, Gaz. Chim. Ital. 118 (1988) 179–185.
[34] J. Remmelgas, G. Harrison, L.G. Leal, A differential constitutive equation for entangled polymer melts, J. Non-Newtonian Fluid Mech. 80 (1999) 115–134.
[35] G. Ianniruberto, G. Marrucci, Stress tensor and stress-optical law in entangled polymers, J. Non-Newtonian Fluid Mech. 79 (1998) 225–234.